Ocean Science
Discussions
Open Access
EGU

1  # A study on some basic features of seiches, inertial

2  # oscillations and near-inertial internal waves

3  Shengli Chen, Daoyi Chen, Jiuxing Xing

4  Shenzhen Key Laboratory for Coastal Ocean Dynamic and Environment, Graduate School at

5  Shenzhen, Tsinghua University, Shenzhen 518055, China.

6  *Correspondence to*: Jiuxing Xing (jxx2012@sz.tsinghua.edu.cn)

7

8

9

10

11

12

13

14

15

16

17

18

19

20

21

22

Ocean Science
Discussions

Open Access

EGU

23    **Abstract**

24    Some basic features of seiches, inertial oscillations and near-inertial internal waves are investigated by

25    simulating a two-dimensional (x-z) shallow basin initialized by a wind pulse. Two cases with and without

26    the vertical stratification are conducted. For the homogeneous case, seiches and inertial oscillations

27    dominate. We find even modes of seiches disappear, which is attributed to a superposition of two seiches

28    generated at east and west coastal boundaries. They have anti-symmetric elevations and a phase lag of

29    nπ, thus their even modes cancel each other. The inertial oscillation shows typical opposite currents

30    between surface and lower layers, which is formed by the feedback between barotropic waves and inertial

31    currents. For the stratified case, near-inertial internal waves are generated are generated at land

32    boundaries and propagate offshore with increasing frequencies, which induce tilting of velocity contours

33    in the thermocline.

34    The inertial oscillation is uniform across the whole basin, except near the coastal boundaries (~20 km)

35    where it quickly declines to zero. This boundary effect is related to great enhancement of nonlinear terms,

36    especially the vertical nonlinear term ( $w\partial\mathbf{u}/\partial z$ ). With inclusion of near-inertial internal waves, the

37    total near-inertial energy has a slight change, with occurrence of a small peak at ~50 km, which is similar

38    to previous researches. We conclude that, for this distribution of near-inertial energy, the boundary effect

39    for inertial oscillations is primary, and the near-inertial internal wave plays a secondary role.

40

41

42

43

44

45

46

47

48

Ocean Science

Discussions

## 1. Introduction

49

50 If a water particle is subject to no force except the Coriolis force, it will move at the local inertial

51 frequency (namely inertial motions). In reality, its frequency is usually slightly biased by other processes

52 (Kunze, 1985). Near-inertial motion has been observed and reported in many seas (e.g. Alford et al.,

53 2016;Webster, 1968). It is mainly generated by changing winds at the sea surface (Pollard and Millard,

54 1970;Chen et al., 2015b). The passage of a cyclone or a front can induce very strong near-inertial

55 motions(D'Asaro, 1985), which can last for 1-2 weeks and reach a maximum velocity magnitude of 0.5-

56 1.0 m/s (Chen et al., 2015a;Zheng et al., 2006;Sun et al., 2011). In deep seas, the near-inertial internal

57 wave propagates downwards to transfer energy to depth (Leaman and Sanford, 1975;Fu, 1981;Gill,

58 1984;Alford et al., 2012). The strong vertical shear of near-inertial currents may play an important role

59 in inducing mixing across the thermocline (Price, 1981;Burchard and Rippeth, 2009).

60 In shelf seas, near-inertial motions exhibit a two-layer structure, with an opposite phase between currents

61 in the surface and lower layers (Malone, 1968;Millot and Crepon, 1981;MacKinnon and Gregg, 2005).

62 By solving a two-layer analytic model using the Laplace transform, Pettigrew (1981) found this

63 'baroclinic' structure can be formed by inertial oscillations without inclusion of near-inertial internal

64 waves. Therefore, due to similar vertical structure and frequencies, inertial oscillations and near-inertial

65 internal waves are hardly separable, and could easily be mistakenly recognized as each other.

66 In shelf seas, the near-inertial energy increases gradually offshore, and reaches a maximum near the shelf

67 break, found both in observations (Chen et al., 1996) and model simulations (Xing et al., 2004;Nicholls

68 et al., 2012). Chen and Xie (1997) reproduced this cross-shelf variation both in linear and nonlinear

69 simulations, and attribute it to large values of the cross-shelf gradient of surface elevation and the vertical

70 gradient of Reynolds stress near the shelf break. By using the analytic model of Pettigrew (1981),

71 Shearman (2005) argued that the cross-shelf variation is controlled by baroclinic waves which emanate

72 from the coast to introduce nullifying effects on the near-inertial energy near shore. Kundu et al. (1983)

73 found a coastal inhibition of near-inertial energy within the Rossby radius from the coast, which is

74 attributed to the downward and offshore leakage of near-inertial energy near the coast. As many factors

75 seems to have effects, the mechanism controlling the cross-shelf variation of near-inertial energy seems

76 complicated.

Ocean Science
Discussions

77    During the occurrence of near-inertial motions, the wind force can also easily generate a seiche in close

78    or semi-close basins (de Jong, 2003). A seiche is a standing wave formed in an enclosed or partially

79    enclosed body of water, which has been widely observed in lakes, harbors, bays and seas (Miles,

80    1974;Metzner et al., 2000;Drago, 2009;Breaker et al., 2010). It has a period ranging from several minutes

81    to several hours. In some regions its amplitude can reach several meters (e.g.Wang et al., 1987), which

82    can induce flooding and cause damage to fishery and coastal facilities. In a closed rectangular basin of

83    length L and depth H, the seiche period is given by the Merian's formula:

84
$$T = \frac{2L}{n\sqrt{gH}}$$
(1)

85    where n=1, 2, 3, … is the mode number. Csanady (1973, using the Laplace transform) found that even

86    modes of seiches were absent. However, the absence of even mode seiches has not been reported in

87    observation or model simulations, probably due to irregular topography in reality which makes it difficult

88    to compute the exact period of each mode. And it is not known why even modes disappear from the

89    perspective of physics which we want to explore.

90    In this paper, we try to use simple simulations to investigate some basic properties of the inertial

91    oscillation and the near-inertial internal wave and differences between them. Generation of two-layer

92    structure of inertial oscillations and horizontal distribution of near-inertial energy are investigated in

93    details. The model is simple two-dimensional (x=600 km, z=60 m) and forced by a wind pulse with land

94    boundaries at both two sides. The missing of even mode seiches is also found and interpreted. Two cases

95    with and without vertical stratification are explored. Model settings are introduced in Section 2. In the

96    homogeneous case (Section 3), properties of seiches and inertial oscillations are investigated. In the

97    stratified case (Section 4), we study the difference near-inertial internal waves introduce. Summary and

98    discussion are presented in the final section (Section 5).

99    **2.  Model Settings**

100    Numerical simulations are done by the MIT general circulation model (MITgcm) (Marshall et al., 1997).

101    The model is two-dimensional (i.e., the gradient along y is zero), with 3000 grids in the horizontal (x;

102    $\Delta x$ =200 m) and 30 grids in the vertical (z; $\Delta z$ =2 m). The water depth is uniform (60 m), with east and

103    west boundaries being closed (land). The vertical and horizontal eddy viscosities are assumed constants

**Ocean Science**
Discussions

Open Access

EGU

104    as $5 \times 10^{-4}$ m$^2$/s and 10 m$^2$/s, respectively. The Coriolis parameter is $5 \times 10^{-5}$ s$^{-1}$ (at a latitude of 20.11 °N).

105    The model is forced by a spatially uniform wind which is kept westward and increases from 0 to 0.73

106    N/m$^2$ (corresponding to a wind speed of 20 m/s) for the first three hours and then suddenly stops. The

107    first case has no vertical stratification, while the second one has a stratification of two-layer structure

108    initially. Except stratification all settings of these two cases are the same.

109    **3.   Results without vertical stratification**

110    For the first case without vertical stratification, seiches and inertial oscillations are two dominant

111    processes.

112    **3.1 Seiches**

113    Due to the westward flow driven by the wind, the water level goes up at the west coast and down at the

114    east coast initially (Fig 1). A wave front propagates from each end at the speed of the barotropic wave

115    ($\sqrt{gH}$ = 24 m/s or 87 km/h). As the wind stress and the water depth are uniform across the basin, the

116    elevation at the west is antisymmetric to that at the east (i.e. with the same amplitude but opposite phase).

117    The spectra of elevations is shown in Fig 2. At the inertial frequency, the elevation energy is slightly

118    increased. The most energetic peak is at the first mode of seiches, which is slightly biased by the earth

119    rotation effect. With the rotation, the wave frequency for each mode of seiche is given by (see the

120    Appendix):

121    $$\omega_n^2 = f^2 + \frac{n^2 \pi^2 gH}{L^2}$$    (2)

122    where $f$ is the inertial frequency, $n$ the mode number, $g$ the gravity acceleration, $H$ the water depth, and

123    $L$ the basin width. As in most cases the horizontal scale of a closed basin is relatively small (<200 km),

124    the second term on the right hand side of Eq. (2) is much greater than the inertial frequency term, thus

125    the rotation effect is usually negligible. Here due to a large basin width (600 km), the rotation effect is

126    obvious.

127    The energy of the first mode is minimal at the middle of the basin (i.e., x=300 km) and maximal at two

128    boundaries. The second mode energy is almost negligible. The third mode, which has three nodes, is

129    much more energetic than the second mode. The fourth mode vanishes, while the fifth mode can be seen

**Ocean Science**
Discussions

130    with five nodes although it has relative low energy. In a word, the even modes are absent. In the real

131    world, due to irregular topography, there is uncertainty in computing the exact period of each mode, and

132    the research on higher modes is limited. Csanady (1973, using the Laplace transform) found the even

133    modes of seiches absent. Here we propose an alternative way combining physics and mathematics to

134    interpret this phenomenon.

135    As derived from the appendix, the elevation of a seiche in a closed basin can be given by

136
$$\eta_1 = \cos\frac{n\pi x}{L}(A_1 \cos\omega_n t + A_2 \sin\omega_n t) \tag{3}$$

137    where A1 and A2 are arbitrary constants. As we see in Fig 1, a barotropic wave originates from the east

138    and west boundaries. Each barotropic wave can form a seiche. If the wind stress and the water depth are

139    spatially uniform, the elevation induced by the seiche at the west is antisymmetric to that at the east. The

140    wave generated at each end takes some time to reach the other end ($t_0 = L/\sqrt{gH}$), which causes a phase

141    difference of $n\pi$ between seiches driven at two ends (i.e., $\omega_n t_0 = 2\pi/T \times (L/\sqrt{gH}) = n\pi$). If the seiche

142    generated by the barotropic wave originating at the west boundary is denoted by (3), the seiche generated

143    by the wave from the east boundary is expressed as

144
$$\eta_2 = \cos\frac{n\pi x}{L}\left[-A_1 \cos(\omega_n t + n\pi) - A_2 \sin(\omega_n t + n\pi)\right] \tag{4}$$

145    The superposition of these two seiches is

146
$$\eta_1 + \eta_2 = \cos\frac{n\pi x}{L}\left[A_1 \cos\omega_n t\left(1 - \cos n\pi\right) + A_2 \sin\omega_n t\left(1 - \cos n\pi\right)\right] \tag{5}$$

147    The odd modes, i.e., n=1, 3, 5…, are amplified:

148
$$\eta_1 + \eta_2 = \cos\frac{n\pi x}{L}\left(2A_1 \cos\omega_n t + 2B_1 \sin\omega_n t\right) \quad (n=1,3,5...) \tag{6}$$

149    The even modes, i.e., n=2, 4, 6…, cancel each other:

150
$$\eta_1 + \eta_2 = 0 \quad (n=2,4,6...) \tag{7}$$

151    Therefore, even modes of seiches cancel each other.

152

### 3.2 Inertial oscillations

153

### 3.2.1 Vertical structures

154

155    The model simulated velocities (Fig. 3) vary near the inertial period (34.9 hours). Since the vertical

156    stratification is absent, this near-inertial motion is pure inertial oscillations. Spectra of velocities (not

157    shown) indicate maximum peaks located exactly at the inertial period. The spectra of u also have a

158    smaller peak at the frequency of the first mode seiche. As this simulation is two-dimensional, i.e., the

159    gradient along $y$-axis is zero, the seiche has little energy in v which shows clearly regular variation at the

160    inertial frequency.

161    In the vertical direction, currents display a two-layer structure, with their phase being opposite between

162    surface and lower layers. They are maximum at the surface, and have a weaker maximum in the lower

163    layer (~40 m), with a minimum at the depth of ~20 m.    The velocity gradually diminishes to zero at the

164    bottom due to the bottom friction. This is the typical vertical structure of shelf-sea inertial oscillations,

165    which have been frequently observed (Shearman, 2005;e.g., MacKinnon and Gregg, 2005). In practice,

166    this vertical distribution can be modified due to presence of other processes, such as the surface maximum

167    being pushed down to the subsurface (e.g. Chen et al., 2013). Note that without stratification in this

168    simulation the near-inertial internal wave is absent. However, this two-layer structure of inertial

169    oscillations looks 'baroclinic', which makes it easy to be mistakenly attributed to the near-inertial internal

170    wave (Pettigrew, 1981).

171    It is interesting that currents of non-baroclinic inertial oscillations reverse between the surface and lower

172    layers. This is usually attributed to the presence of the coast, which requires the normal-to-coast transport

173    to be zero, thus currents in upper and lower layers compensate each other (Millot and Crepon, 1981;Chen

174    et al., 1996). Here we try to give more detail on how this process works.

175    As the westward wind blows for first three hours, the initial inertial current is also westward and only

176    exists in the very surface layer (Fig. 4). In the lower layer there is no movement initially. Thus a westward

177    transport is produced, which generates a rise (in the west) and fall (in the east) of elevation near coastal

178    boundaries. The elevation slope behaves in a form of barotropic wave which propagates offshore at a

179    great speed (87 km/h). The current driven by the barotropic wave is eastward, and uniform vertically.

180    Therefore, with arrival of the barotropic wave the westward current in the surface is reduced, and the

Ocean Science
Discussions

181  movement in the lower layer commences (Fig. 4). After passage of the first two barotropic waves

182  (originated from both sides), currents in the lower layer have reached a relatively great value, while

183  currents in the surface layer have been largely decreased (Fig. 5a). Accordingly, the depth-integrated

184  transport diminishes a lot. This is like a feedback between inertial currents and barotropic waves. If only

185  the depth-integrated transport of currents exist, barotropic waves will be generated, which reduce the

186  surface currents but increase the lower layer currents, thus reduces the current transport. It will end up

187  with inertial currents in the surface and lower layers having opposite directions and comparable

188  amplitudes. As seen from Fig. 3b, the typical vertical structure of inertial currents is established within

189  the first inertial period. At a place further offshore, such as at x=200 km, the barotropic wave takes about

190  two more hours to arrive compared with x=70 km, thus the maximum value of inertial currents in lower

191  layer is lagged behind that in surface layer (Fig. 5b).

192  **3.2.2 Horizontal distributions of inertial energy**

193  The inertial velocities are almost entirely the same across the basin (Fig. 6), except near the boundary.

194  This indicates that inertial oscillations have a coherence scale of almost the basin width. This is because

195  in our simulation the wind force is spatially uniform, and the bottom is flat. The inertial velocities in the

196  lower layer have slightly more variation across the basin than those in the surface layer, because inertial

197  velocities in the lower layer is correlated to propagation of barotropic waves as discussed in 3.2.1, while

198  the surface inertial currents are driven by spatially uniform wind. In shelf sea regions, the wind forcing

199  is usually coherent as the synoptic scale is much larger, however, the topography that is mostly not flat

200  could generate barotropic waves at various places, and thus significantly decrease coherence of inertial

201  currents in the lower layer.

202  The spectra of velocities in the inertial band are almost uniform except near the boundaries (Fig. 7),

203  consistent with the velocities. Near the boundaries, the inertial energy declines gradually to zero from

204  x=~20 km to the coast wall. The east side has slightly greater inertial energy and a bit wider boundary

205  layer compared to the west side.

206  We calculate the nonlinear and inertial terms in the momentum equation and find that nonlinear terms

207  are of relatively high values initially within 2 km away from the land boundary (Fig 8bc), where the

208  inertial term is smaller (Fig 8a). For the time-averaged values (Fig 8d), the vertical nonlinear term is two

Ocean Science
Discussions
Open Access
EGU

209    times more than the horizontal nonlinear term. The inertial term drops sharply near the boundary, and

210    rises gradually with the distance away from the boundary. At x> 15km, it keeps an almost constant value

211    which is much greater than nonlinear terms. Thus it is concluded that the significant decrease of inertial

212    oscillations near the boundary is due to influence of nonlinear terms, especially the vertical nonlinear

213    term.

214    **4.   Near-inertial internal waves**

215    In addition to inertial oscillations, near-inertial internal waves are usually generated along when the

216    vertical stratification is present. However, due to their close frequencies inertial oscillations and near-

217    inertial internal waves are difficult to be separated. Thus we run a second simulation with the presence

218    of stratification to investigate differences that near-inertial internal waves introduce. The temperature is

219    20 ℃ in the upper layer (-30 m<z<0), and 15 ℃ in the lower layer (-60 m<z<-30 m). The salinity is

220    constant, so the density is determined by the temperature.

221    **4.1 Temperature distributions**

222    Fig. 9 shows the evolution of temperature profiles with time. One can see an internal wave packet is

223    generated at the west coast, and then propagates offshore. The wave phase speed is around 1 km/h,

224    consistent with the theoretical value computed using the stratification. Before arrival of internal waves,

225    the temperature at mid-depth diffuses gradually due to vertical diffusion in the model. For a fixed position

226    at x=20 km (Fig. 10), the temperature varies with the inertial period (34.9 hours) and the amplitude of

227    fluctuation declines gradually with time. At x=60 km and x=100 km, the strength of internal waves is

228    much reduced. And wave periods are shorter initially, followed by a gradually increase to the inertial

229    period. At x=140 km, the internal wave becomes as weak as the background disturbance.

230    A spectral analysis of the temperature at mid-depth (z=-30 m) is shown in Fig. 11a. The strongest peak

231    is at near the inertial frequency (0.69 cpd), but only confined to the region close to the boundary (x<40

232    km). In the region 20km<x<70km, the energy is also large at higher frequencies of 0.8-1.7 cpd. This

233    generally agrees with properties of Poincaré waves. During a Rossby adjustment, the waves with higher

234    frequencies propagate offshore at greater group speeds, thus for places further offshore the waves have

235    higher frequencies (Millot and Crepon, 1981). While the wave with a frequency closest to the inertial

236    frequency moves at the slowest group velocity, and it takes a relatively long time to propagate far offshore,

Ocean Science
Discussions

237 thus it is mostly confined to near the boundary. By solving an idealized two-layer model equation, the

238 response of Rossby adjustment can be expressed in form of Bessel functions (Millot and Crepon,

239 1981;Gill, 1982;Pettigrew, 1981), as in Fig. 11cd showing the spectra of mid-depth elevation. The

240 difference from our case is obvious. The frequency of theoretical near-inertial waves increase gradually

241 with the distance from the coast, while in our case this property is absent. And the theoretical inertial

242 energy has a e-folding scale of almost the Rossby radius (54 km), while in our case the e-folding scale is

243 much smaller (~15 km).

244 **4.2 Velocity distributions**

245 With presence of near-inertial internal waves, the contours of velocities near the thermocline tilt slightly

246 (Fig. 12d), and indicates an upward propagation of phase, thus a downward energy flux. This can also be

247 seen in vertical spirals of velocities (Figs. 12e and 12f). With only inertial oscillations, current vectors

248 mostly point toward two opposite directions. Once the near-inertial wave is included, the current vectors

249 gradually rotate clockwise with depth.

250 The spatial distribution of the near-inertial energy is also slightly changed compared to the case with only

251 inertial oscillations (Fig. 13 and Fig. 7). It is also greatly reduced to zero in the boundary layer (0-20 km)

252 like the case without stratification. But at ~50 km away from the boundary the inertial energy reaches a

253 peak. Further away (>100 km) it becomes a constant. This spatial distribution of inertial energy is similar

254 to that observed in shelf seas, with maximum near the shelf break (Chen et al., 1996;Shearman, 2005).

255 In our case, the boundary layer effect which induces a sharp decrease to zero makes a major contribution,

256 and near-inertial internal waves which bring a small peak further offshore make a secondary influence.

257 **5.   Summary and discussion**

258 Two sets of idealized simple two-dimensional (x-z) simulations are conducted to examine the response

259 of a shallow closed basin (600 km×60 m) to a wind pulse. The first case is homogeneous, in which

260 properties of seiches and inertial oscillations are investigated. Barotropic waves are generated at two

261 coastal boundaries which then propagate and reflect to form seiches. The seiche has the horizontal

262 structure and frequencies consistent with the theory. Seiches of even-number modes are absent, which

263 has been rarely reported. By using the Laplace transform to solve the equations, Csanady (1973) found

264 even mode seiches absent. We interpret it as superposition of two seiches, which are formed by barotropic

Ocean Science

Discussions

Open Access

265   waves originating from east and west boundaries. They have anti-symmetric elevation and a phase lag

266   of nπ, thus their even mode cancels each other. The mechanism we propose is more physical, and thus a

267   good supplement to explain this phenomenon. Note that for the even modes to be absent the wind forcing

268   and the topography are required to be uniform spatially to keep these two seiches having anti-symmetric

269   elevation.

270   The inertial oscillation is energetic in the homogeneous case. It has a two-layer structure, with currents

271   in the surface and lower layers being opposite in phase, which has been reported frequently in shelf seas.

272   We find that the inertial current is confined in the surface layer initially. The induced depth-integrated

273   transport generates barotropic waves near boundaries which propagates quickly offshore. The flow

274   driven by the barotropic wave is independent of depth and opposite to the surface flow. Thus the surface

275   flow is reduced but the flow in the lower layer is increased, as a result the transport diminishes. This

276   feedback between barotropic waves and currents continues and ends up with the depth-integrated

277   transport vanishes, i.e., inertial currents in upper and low layers having opposite phases and comparable

278   amplitudes. In our simulation, within just one inertial period the typical structure of inertial currents has

279   been established. By solving a two-layer analytic model using the Laplace transform, Pettigrew (1981)

280   also found the vertical structure of opposite currents associated with inertial oscillations. He argued that

281   the arrival of a barotropic wave for a fixed location cancels half of the inertial oscillation in the surface

282   layer, and initiates an equal and opposite oscillation in the lower layer. Our simulations further

283   demonstrate the role of barotropic waves in forming this feature, and shows some more realistic details

284   during this process.

285   The second case is set up with idealized two-layer stratification, thus near-inertial internal waves are

286   generated. For a fixed position, velocity contours clear obvious tilting near the thermocline, and velocity

287   vectors display clearly anti-cyclonic spirals with depth. These could be useful clues to examine

288   occurrence of near-inertial internal waves. Near the land boundary the vertical elevation generates

289   fluctuations of thermocline that propagate offshore. The energy of near-inertial internal waves is confined

290   to near the land boundary (x< 40 km). At positions further offshore, the waves have higher frequencies.

291   This is generally consistent with properties of Rossby adjustment process. However, our simulated result

292   also shows evident discrepancies from theoretical values obtained in classic solutions of Rossby

293   adjustment problem.

Ocean Science
Discussions

294    The inertial oscillation has a very large coherent scale of almost the basin scale (600 km). It is uniform

295    in both amplitude and phase across the basin, except near the boundary (~20 km offshore). The energy

296    of inertial oscillations declines gradually to zero from x=20 km to the coast. This boundary effect is

297    attributed to influence of nonlinear terms, especially the vertical term ( $w\partial\mathbf{u}/\partial z$ ), which are greatly

298    enhanced near the boundary, and overweighs the inertial term ( $f\mathbf{u}$ ). When near-inertial internal waves

299    are produced in the stratified case, the distribution of total near-inertial energy is modified slightly near

300    the boundary. A small peak appears at ~ 50 km offshore. This is similar to the cross-shelf distribution of

301    near-inertial energy observed in shelf seas (Chen et al., 1996;Shearman, 2005). This energy distribution

302    has been attributed to different reasons, such as downward and offshore leakage of near-inertial energy

303    near the coast (Kundu et al., 1983), the variation of elevation and Reynolds stress terms associated with

304    the topography (Chen and Xie, 1997) and the influence of the baroclinic wave (Shearman, 2005;Nicholls

305    et al., 2012). In our simulations, this horizontal distribution of near-inertial energy is primarily controlled

306    by the boundary effect on inertial oscillations, and the near-inertial internal wave makes a secondary

307    effect.

308

309

310

311    **Acknowledgements**

317

318

319

**Ocean Science**
Discussions

Open Access

320                  **Appendix: the derivation for the general solution of seiches**

321    The governing equations for seiches can be simplified as:

322
$$\frac{\partial u}{\partial t} - fv = -g\frac{\partial \eta}{\partial x} \qquad (A1a)$$

323
$$\frac{\partial v}{\partial t} + fu = 0 \qquad (A1b)$$

324
$$\frac{\partial \eta}{\partial t} + H\frac{\partial u}{\partial x} = 0 \qquad (A1c)$$

325    where u and v are eastward and northward velocities, $\eta$ the elevation, $f$ the inertial frequency, $g$ the gravity

326    acceleration, $H$ the water depth. Substitutions of $\eta$ and $v$ by $u$ give

327
$$\frac{\partial^2 u}{\partial t^2} + f^2 u - gH\frac{\partial^2 u}{\partial x^2} = 0 \qquad (A2)$$

328    If we assume

329
$$u = X(x)T(t) \qquad (A3)$$

330    and substitute (A3) in (A2), we get

331
$$\frac{T''}{T} + f^2 = \frac{gHX''}{X} \qquad (A4)$$

332    If a function of $t$ equals a function of $x$, they have to both equal a constant,

333
$$\frac{T''}{T} + f^2 = \frac{gHX''}{X} = -C \qquad (A5)$$

334    The equation of $x$ is then given by

335
$$gHX'' + CX = 0 \qquad (A6)$$

336    The solution of (A6) can be readily obtained

Ocean Science

Discussions

Open Access

EGU

337
$$X = C_1 \sin \sqrt{\frac{C}{gH}} x + C_2 \cos \sqrt{\frac{C}{gH}} x \quad (C > 0) \quad \text{(A7)}$$

338    where $C_1$ and $C_2$ are arbitrary constants. The across-coast velocity must vanish at boundaries, i.e., u=0 at

339    x=0, L, thus

340
$$X = C_1 \sin \sqrt{\frac{C}{gH}} x \quad \text{(A8a)}$$

341
$$C = \frac{n^2 \pi^2 gH}{L^2} \quad \text{(A8b)}$$

342    The solution for $T$ is then

343
$$T = C_3 \sin \omega_n t + C_4 \cos \omega_n t \quad \text{(A9a)}$$

344
$$\omega_n^2 = f^2 + \frac{n^2 \pi^2 gH}{L^2} \quad \text{(A9b)}$$

345    where $C_3$ and $C_4$ are arbitrary constants. Therefore the solution for $u$ is

346
$$u = C_1 \sin \frac{n\pi x}{L} \left( C_3 \sin \omega_n t + C_4 \cos \omega_n t \right) \quad \text{(A10a)}$$

347    and the solutions for of $\eta$ and $v$ are

348
$$\eta = C_1 \frac{n\pi H}{\omega_n L} \cos \frac{n\pi x}{L} \left( C_3 \cos \omega_n t - C_4 \sin \omega_n t \right) \quad \text{(A10b)}$$

349
$$v = C_1 \frac{f}{\omega_n} \sin \frac{n\pi x}{L} \left( C_3 \cos \omega_n t - C_4 \sin \omega_n t \right) \quad \text{(A10c)}$$

350

351

352

353

354 **References**

355 Alford, M. H., Cronin, M. F., and Klymak, J. M.: Annual Cycle and Depth Penetration of Wind-Generated

356 Near-Inertial Internal Waves at Ocean Station Papa in the Northeast Pacific, Journal of Physical

357 Oceanography, 42, 889-909, 10.1175/jpo-d-11-092.1, 2012.

358 Alford, M. H., MacKinnon, J. A., Simmons, H. L., and Nash, J. D.: Near-Inertial Internal Gravity Waves in

359 the Ocean, Ann Rev Mar Sci, 8, 95-123, 10.1146/annurev-marine-010814-015746, 2016.

360 Breaker, L. C., Tseng, Y.-h., and Wang, X.: On the natural oscillations of Monterey Bay: Observations,

361 modeling, and origins, Progress in Oceanography, 86, 380-395, 10.1016/j.pocean.2010.06.001, 2010.

362 Burchard, H., and Rippeth, T. P.: Generation of Bulk Shear Spikes in Shallow Stratified Tidal Seas,

363 Journal of Physical Oceanography, 39, 969-985, 10.1175/2008jpo4074.1, 2009.

364 Chen, C., and Xie, L.: A numerical study of wind-induced, near-inertial oscillations over the Texas-

365 Louisiana shelf, Journal of Geophysical Research: Oceans, 102, 15583-15593, 10.1029/97jc00228,

366 1997.

367 Chen, C. S., Reid, R. O., and Nowlin, W. D.: Near-inertial oscillations over the Texas Louisiana shelf, J

368 Geophys Res-Oceans, 101, 3509-3524, 10.1029/95jc03395, 1996.

369 Chen, G., Xue, H., Wang, D., and Xie, Q.: Observed near-inertial kinetic energy in the northwestern

370 South China Sea, J Geophys Res-Oceans, 118, 4965-4977, 10.1002/jgrc.20371, 2013.

371 Chen, S., Hu, J., and Polton, J. A.: Features of near-inertial motions observed on the northern South

372 China Sea shelf during the passage of two typhoons, Acta Oceanologica Sinica, 34, 38-43,

373 10.1007/s13131-015-0594-y, 2015a.

374 Chen, S., Polton, J. A., Hu, J., and Xing, J.: Local inertial oscillations in the surface ocean generated by

375 time-varying winds, Ocean Dynamics, 65, 1633-1641, 10.1007/s10236-015-0899-6, 2015b.

376 Csanady, G. T.: Transverse internal seiches in large oblong lakes and marginal seas, Journal of Physical

377 Oceanography, 3, 439-447, 10.1175/1520-0485(1973)003<0439:tisilo>2.0.co;2, 1973.

378 D'Asaro, E. A.: The energy flux from the wind to near-inertial motions in the surface mixed layer,

379 Journal of Physical Oceanography, 15, 1043-1059, 1985.

380 de Jong, M. P. C.: Generation of seiches by cold fronts over the southern North Sea, Journal of

381 Geophysical Research, 108, 10.1029/2002jc001422, 2003.

382 Drago, A.: Sea level variability and the 'Milghuba' seiche oscillations in the northern coast of Malta,

383 Central Mediterranean, Physics and Chemistry of the Earth, Parts A/B/C, 34, 948-970,

384 10.1016/j.pce.2009.10.002, 2009.

385 Fu, L. L.: Observations and models of inertial waves in the deep ocean, Reviews of Geophysics, 19,

386 141-170, 10.1029/RG019i001p00141, 1981.

387 Gill, A. E.: Atmosphere-ocean dynamics, Academic Press, 662 pp., 1982.

388 Gill, A. E.: On the behavior of internal waves in the wakes of storms, Journal of Physical Oceanography,

389 14, 1129-1151, 10.1175/1520-0485(1984)014<1129:otboiw>2.0.co;2, 1984.

390 Kundu, P. K., Chao, S. Y., and McCreary, J. P.: Transient coastal currents and inertio-gravity waves, Deep-

391 Sea Research Part a-Oceanographic Research Papers, 30, 1059-1082, 10.1016/0198-0149(83)90061-4,

392 1983.

393 Kunze, E.: Near-inertial wave propagation in geostrophic shear, Journal of Physical Oceanography, 15,

394 22, 1985.

395 Leaman, K. D., and Sanford, T. B.: Vertical energy propagation of inertial waves: a vector spectral

396 analysis of velocity profiles, Journal of Geophysical Research, 80, 1975-1978, 1975.

397 MacKinnon, J. A., and Gregg, M. C.: Near-inertial waves on the New England shelf: The role of evolving

Ocean Science
Discussions

398   stratification, turbulent dissipation, and bottom drag, Journal of Physical Oceanography, 35, 2408-
399   2424, 10.1175/jpo2822.1, 2005.
400   Malone, F. D.: An analysis of current measurements in Lake Michigan, Journal of Geophysical
401   Research, 73, 7065-&, 10.1029/JB073i022p07065, 1968.
402   Marshall, J., Adcroft, A., Hill, C., Perelman, L., and Heisey, C.: A finite-volume, incompressible Navier
403   Stokes model for studies of the ocean on parallel computers, Journal of Geophysical Research: Oceans,
404   102, 5753-5766, 10.1029/96jc02775, 1997.
405   Metzner, M., Gade, M., Hennings, I., and Rabinovich, A. B.: The observation of seiches in the Baltic Sea
406   using a multi data set of water levels, Journal of Marine Systems, 24, 67-84, 10.1016/s0924-
407   7963(99)00079-2, 2000.
408   Miles, J. W.: Harbor seiching, Annual Review of Fluid Mechanics, 6, 17-35,
409   10.1146/annurev.fl.06.010174.000313, 1974.
410   Millot, C., and Crepon, M.: Inertial oscillations on the continental-shelf of the Gulf of Lions -
411   observations and theory, Journal of Physical Oceanography, 11, 639-657, 10.1175/1520-
412   0485(1981)011<0639:iootcs>2.0.co;2, 1981.
413   Nicholls, J. F., Toumi, R., and Budgell, W. P.: Inertial currents in the Caspian Sea, Geophysical Research
414   Letters, 39, 10.1029/2012gl052989, 2012.
415   Pettigrew, N. R.: The dynamics and kinematics of the coastal boundary layer off Long Island, 1981.
416   Pollard, R. T., and Millard, R. C.: Comparison between ovserved and simulated wind-generated inertial
417   oscillations, Deep Sea Research, 813-821, 1970.
418   Price, J. F.: Upper ocean response to a hurricane, Journal of Physical Oceanography, 11, 153-175,
419   10.1175/1520-0485(1981)011<0153:uortah>2.0.co;2, 1981.
420   Shearman, R. K.: Observations of near-inertial current variability on the New England shelf, Journal of
421   Geophysical Research, 110, 10.1029/2004jc002341, 2005.
422   Sun, Z., Hu, J., Zheng, Q., and Li, C.: Strong near-inertial oscillations in geostrophic shear in the
423   northern South China Sea, Journal of Oceanography, 67, 377-384, 10.1007/s10872-011-0038-z, 2011.
424   Wang, X. Z., Li, K. P., Yu, Z. W., and Wu, J.: Statistical characteristics of seiches in Longkou harbor,
425   Journal of Physical Oceanography, 17, 1063-1065, 10.1175/1520-0485(1987)017<1063:scosil>2.0.co;2,
426   1987.
427   Webster, F.: Observation of inertial period motions in the deep sea, Reviews of Geophysics, 6, 473-
428   490, 1968.
429   Xing, J. X., Davies, A. M., and Fraunie, P.: Model studies of near-inertial motion on the continental
430   shelf off northeast Spain: A three-dimensional two-dimensional one-dimensional model comparison
431   study, J Geophys Res-Oceans, 109, 10.1029/2003jc001822, 2004.
432   Zheng, Q., Lai, R. J., and Huang, N. E.: Observation of ocean current response to 1998 Hurricane
433   Georges in the Gulf of Mexico, Acta Oceanol. Sin., 25, 1-14, 2006.
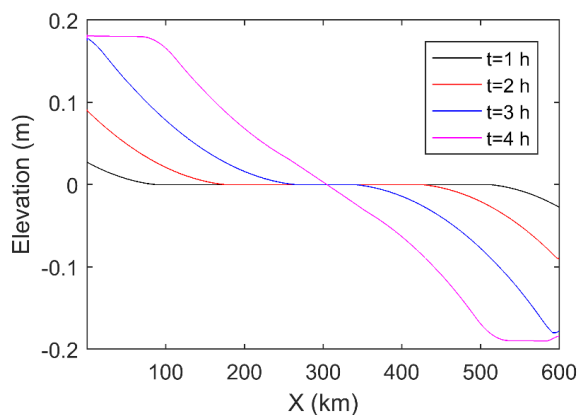
434

435

436

437

Ocean Science
Discussions

Open Access

EGU

438 **Figures**

439



440

441                          Fig 1. Elevation varying in the first 4 hours.
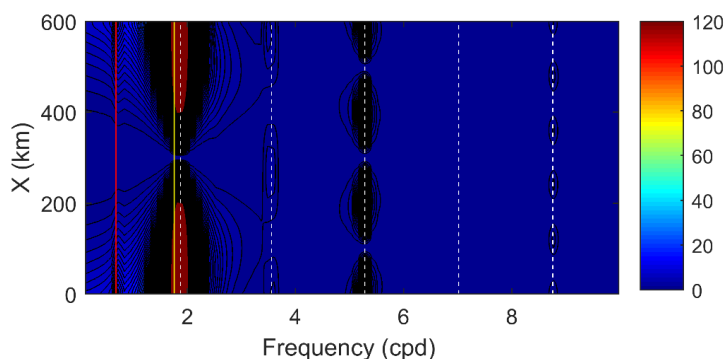
442



443

444        Fig 2. Elevation power spectral density (m$^2$s) dependence with x direction. The red line denotes the

445    inertial frequency, and the yellow line is the frequency of first mode seiche without the rotation effect.

446      The white dash lines are frequencies of first five modes of seiches computed by Eq. (2). The contour

447                                        interval is 1 m$^2$s.

448

Ocean Science

Discussions

Open Access

449
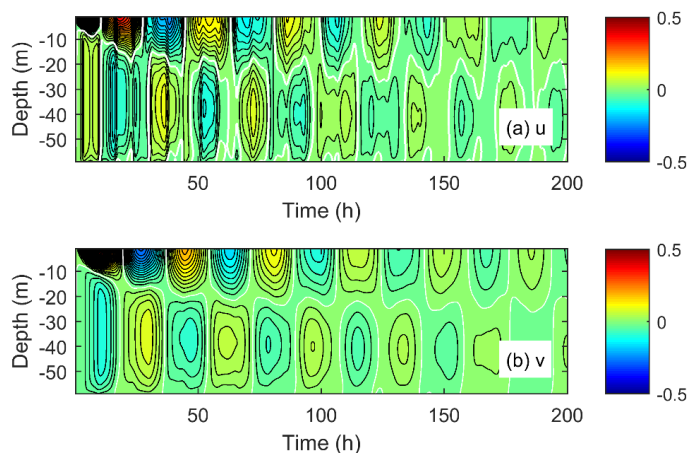
Fig. 3 Velocities (u and v, m/s) at x=70 km. The white lines denote the value of zero. The contour

interval is 0.02 m/s for both panels.

452

453
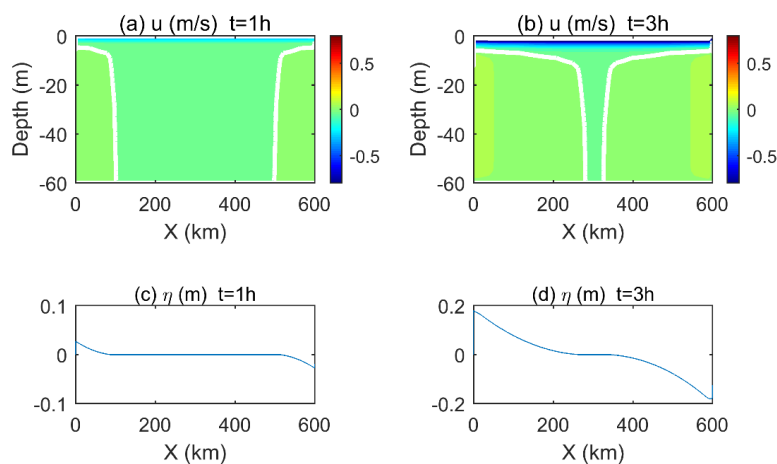
Fig. 4 Snapshots of eastward velocity and elevation ($\eta$) at t=1 and 3 hour. The white lines represent the

value of zero.

456

Ocean Science
Discussions

Open Access



457
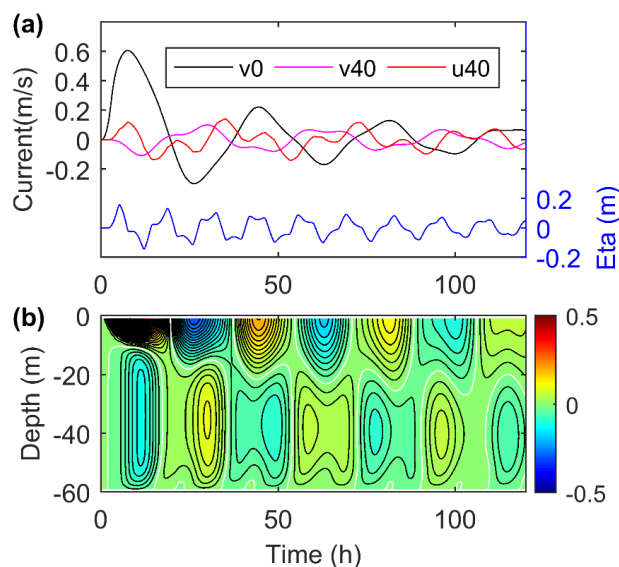
Fig. 5 (a) Time series of velocities and elevation at x=200 km. 'v0' and 'v40' mean the northward

velocity (v) at depths of 0 m and 40 m, and 'u40' is the eastward velocity (u) at 40 m. (b) Contours of v

at x=200 km. The white lines denote the value of zero, and the contour interval is 0.02 m/s.

461



462
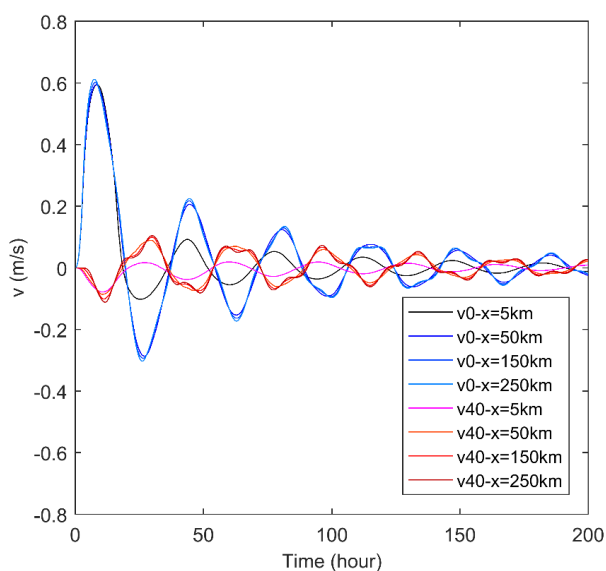
463    Fig. 6 Time series of the northward velocity (v) at different depths and positions. 'v0' and 'v40' mean v

464                                at depths of 0 m and 40 m.

465

466



467
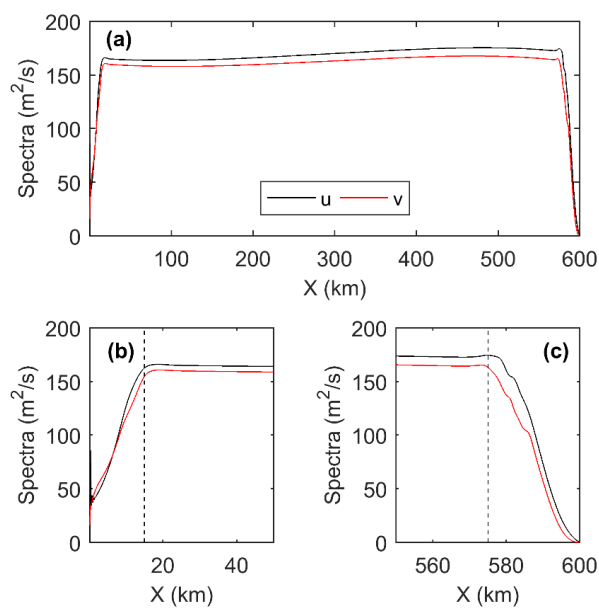
468    Fig. 7 Spatial variation of spectra of velocities in near-inertial band for the homogeneous case. (b) and

469                                (c) display detailed values near boundaries.
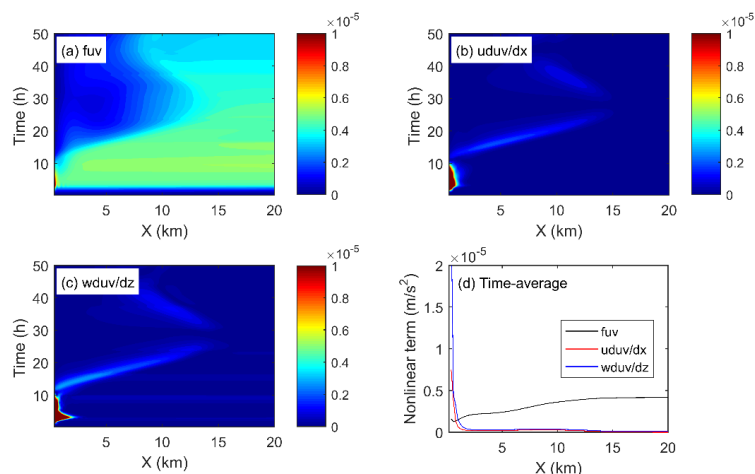
470

Ocean Science
Discussions

Open Access

471



472    Fig 8. Variation of depth-mean inertial and nonlinear terms (m/s²). The inertial term (a) is calculated as

473    $\left| f(u+iv) \right|$, the horizontal nonlinear term (b) is $\left| u\left( \partial u / \partial x + i\partial v / \partial x \right) \right|$, and the vertical nonlinear

474    term (c) is $\left| w\left( \partial u / \partial z + i\partial v / \partial z \right) \right|$. (d) Time averaged value for the first 50 hours.
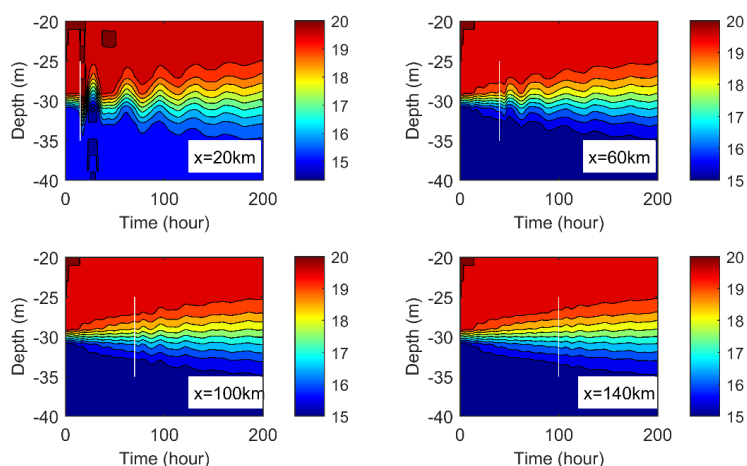
475



476
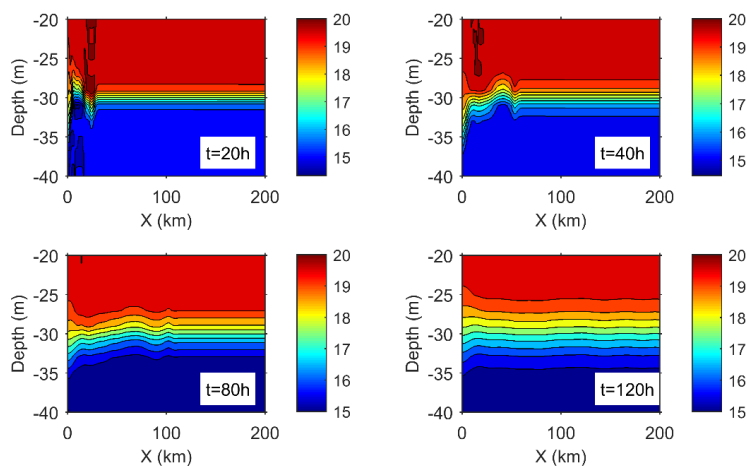
477    Fig. 9 Snapshots of temperature profiles at t=20h, 40h, 80h and 120h. The contour interval is 0.5 ℃.
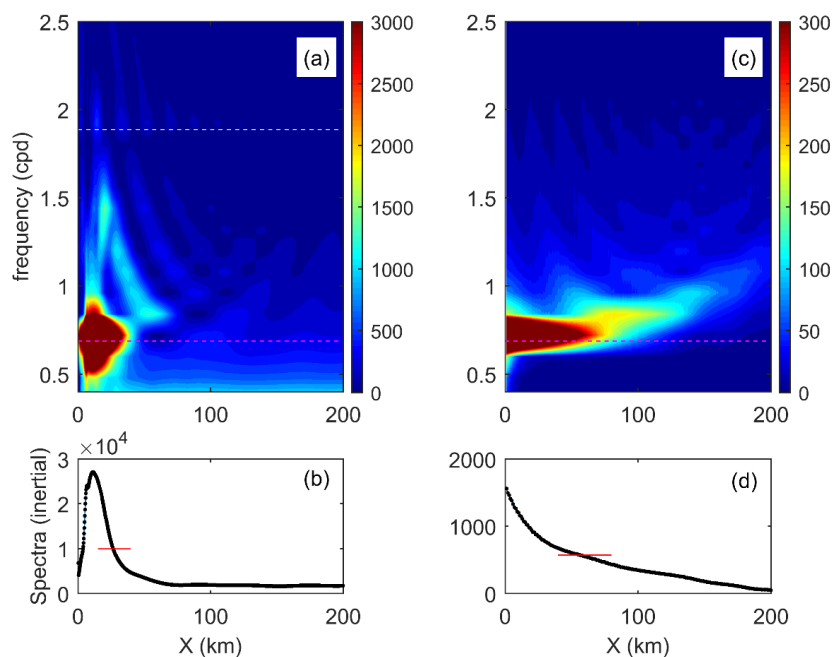
478

Fig. 10 Time series of temperature at x=20, 60, 100 and 140 km. White lines denote arrival of internal

waves. The contour interval is 0.5 ℃.



Fig. 11 (a) Spectra of the temperature at the mid-depth (z=-30 m). The pink dash line represents the

**Ocean Science**
Discussions

485    inertial frequency, and the white line is the first mode seiche frequency. (b) Sum of spectra in inertial

486    band with a red line denoting the e-folding value of the peak. (c) Theoretical spectra of mid-depth

487    elevation calculated from the solution in the form of a Bessel function as in Eq. 3.16 of Pettigrew

488                        (1981). (d) Same as (b) but for theoretical spectra.
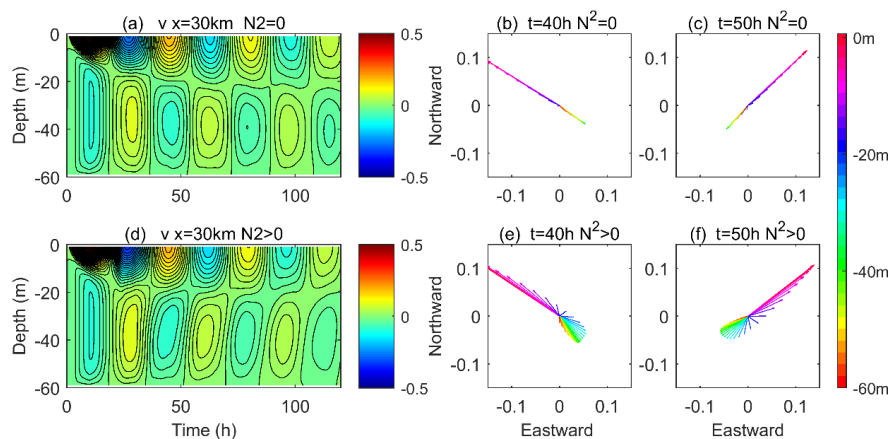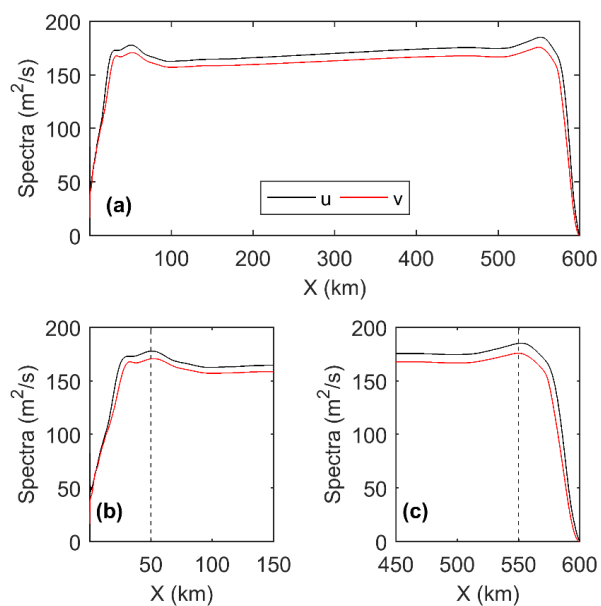
489



490

491    Fig. 12 Distribution of velocity v (m/s) and current spirals for the cases without (a, b, c) and with (d, e,

492                        f) stratification at x=30 km. The contour interval is 0.02 m/s.

493

Ocean Science

Discussions

Open Access

EGU

494

495     Fig. 13 Spatial variation of spectra of velocities in near-inertial band for the stratified case. (b) and (c)

496                         display detailed values near boundaries.